Zinc electrodeposition from a chloride-free non-aqueous solution based on ethylene glycol and acetate salts

G. Panzeri [a], D. Muller [b], A. Accogli [a], E. Gibertini [a], E. Mauri [a], F. Rossi [a], L. Nobili [a], L. Magagnin [a, *]

[a] *Dipartimento di Chimica, Materiali e Ingegneria Chimica Giulio Natta, Politecnico di Milano, 20131 Milano, Italy*
[b] *ETH Zürich, Zürich, Switzerland*

ABSTRACT

In this work, the electrodeposition of zinc is carried out from a chlorides-free organic solution based on ethylene glycol (EG) and acetate precursor salts. The formation of an EG-complex with zinc was observed through ^{1}H NMR. The electrochemical characterization was performed by means of cyclic voltammetry (CV) and linear sweep voltammetry (LSV) on platinum and steel respectively. Electrodeposition was investigated with both potentiostatic (from −1 V vs Pt to −2 V vs Pt) and galvanostatic (from −2 mA/cm^2 to −16 mA/cm^2) approaches together with Hull cell test: cathodic efficiencies > 85% were reported. Scanning electron microscopy (SEM) and X-ray diffraction (XRD) analyses showed that the films were compact, with large grains and a hexagonal microstructure preferentially oriented along the [002]/[102] directions. The high purity of the deposits was assessed by electron dispersive spectroscopy (EDS). Po-larization tests in de-aerated 5 %wt NaCl solution resulted in a corrosion potential of $E_{corr} = -1.03$ V vs Ag/AgCl ($I_{corr} = 1.01 \times 10^{-6}$ A/cm^2).

Keywords:
Electroplating
Zinc
Organic Solvent
NMR
DES
Hull

1. Introduction

Since the discovery of non-aqueous electrolytes and their applicability to electrodeposition, zinc and zinc alloys have been among the most studied plating systems. The low reduction potential of zinc may consist in a limit considering the traditional aqueous solutions because of the unavoidable water electrolysis. Together with a lower efficiency, hydrogen evolution can also be responsible for embrittlement phenomena with a consequent change in the mechanical properties [1,2]. The adoption of non-aqueous solutions is indeed a valid alternative to limit secondary reactions and to potentially obtain high-quality [3–7]. However, there are also drawbacks affecting this organic media as the lower metals solubility or the lower solution conductivity, resulting in higher energy consumption. At the industrial level, electrolyte drag-out due to the significant bath viscosity together with the relatively high cost of the organic solvents/electrolyte are one of the main problems to be solved. Moreover, long-term stability of the bath should be also guaranteed, evaluating both cathodic and anodic secondary reactions [8–10]. In the last decades, zinc electrodeposition has been investigated in many non-aqueous media mainly belonging to ionic liquids (ILs) [11–20] and deep eutectic solvents (DESs) [21–31]. In the former one, the organic solvent employed acts also as electrolyte [3] while in the latter a hydrogen bond donor (HBD) is mixed in a proper molar ratio with a hydrogen bond acceptor (HBA), e.g. quaternary ammonium salt, forming a conductive eutectic solution [4–6]. The latter ones were proposed a decade ago as possible candidate alternative to room temperature ionic liquids (RTIL) whose cost and potential toxicity limited the diffusion to the industrial level [5]. Nowadays, DESs are considered as one of the possible candidates for the replacement of traditional plating solutions and in some cases they have been already scaled up to an industrial level [4,7]. However, the presence of choline chloride in high concentrations in the bath 1ChCl:2X (X = EG, Urea (U)) may result in an aggressive environment towards the substrate and the electrodeposit. Moreover, because of its high hygroscopicity, a long drying procedure is required prior to obtain a DES solution. As a consequence, the elimination or substitution of choline chloride is an option to be considered. In a previous work, we investigated the effect of changing the choline chloride/ethylene glycol molar ratio in the bath on film composition, fixing the other electrodeposition parameters [32]. In more recent times, we have

* Corresponding author.
E-mail address: luca.magagnin@polimi.it (L. Magagnin).

Published Journal Article available at: https://doi.org/10.1016/j.electacta.2018.11.060

demonstrated the possibility to obtain high purity films [33] from a simple ethylene glycol solution containing the precursor salt, limiting the concentration of chlorides of about one/two orders of magnitude with respect to 1ChCl:2EG DES. The final deposits showed a much better corrosion performances than the analogous ones obtained from urea/choline chloride-based DES (1ChCl:2U) [34], demonstrating the effectiveness of this approach. The use of ethylene glycol as solvent containing relatively low concentration of chlorides has been reported by different research groups, showing the suitability of the system for both metals and alloys together with an easier experimental procedure and lower solution cost [33,35–40]. However, along with the progressive reduction of chlorides in the solution, with a less aggressive/corrosive environment towards the electrodeposited film and the surrounding apparatus, a much lower conductivity of the electrolyte was reached. For this reason, alternative precursor salts to chlorides, with high solubility in ethylene glycol, must be considered in order to have an inert environment with good conductivity.

In this work, we propose a novel organic solution based on ethylene glycol together with the use of acetate salts, employed for the first time in an organic plating solution for the best of author's knowledge.

2. Experimental

Anhydrous ethylene glycol (EG) [$C_2H_6O_2$] (Sigma Aldrich 99.8%), zinc acetate ($Zn(OAc)_2$) [$Zn(CH_3COO)_2 \cdot 2H_2O$] (Sigma Aldrich) and sodium acetate (NaOAc) [CH_3COONa] (Sigma Aldrich) were used as received. Ethylene glycol (EG) was kept at 70 °C (vapor pressure $P^\circ = 0.064$ bar) during both solution preparation and electrochemical characterization/electrodeposition using a thermal jacket controlled by a thermocouple. Sodium acetate (0.5 M) was added first, followed by the addition of zinc acetate (0.75 M) once completely dissolved. The NMR experiments were carried out on a Bruker AC (400 MHz) spectrometer using deuterium oxide (D_2O) as solvent and the resulting chemical shifts were reported as δ values in parts per million with respect to tetramethylsilane (TMS) as an internal standard. The electrochemical characterization was carried out in a conventional three-electrode cell equipped with AMEL2550 Potentiostat/Galvanostat. For the cyclic voltammetry (CV), platinum wires, cleaned in regia solution, were chosen as working (WE), counter and pseudo-reference electrodes. No ohmic compensation was performed since the close proximity of the RE to the WE resulted in a negligible potential drop. On the other hand, linear sweep voltammetry (LSV) and potentiostatic depositions (PDs) were carried out on polished iron substrates, previously etched in 10% hydrochloric acid aqueous solution. Galvanostatic depositions (GDs) were carried out in a conventional two-electrodes cell while Hull cell test was carried out in a 33 ml test cell (Tenori Hull-cell) by Yamamoto-MS. After deposition, samples were washed thoroughly with water and acetone, and subsequently dried under nitrogen flux. Films thickness was determined by both X-ray fluorescence (XRF) apparatus Fischerscope X-ray XAN and optical profilometer UBM Microfocus; for both PDs and GDs a charge density of 12 C/cm^2 was selected, resulting in a film thickness ranging from 3 μm to 4 μm depending on the

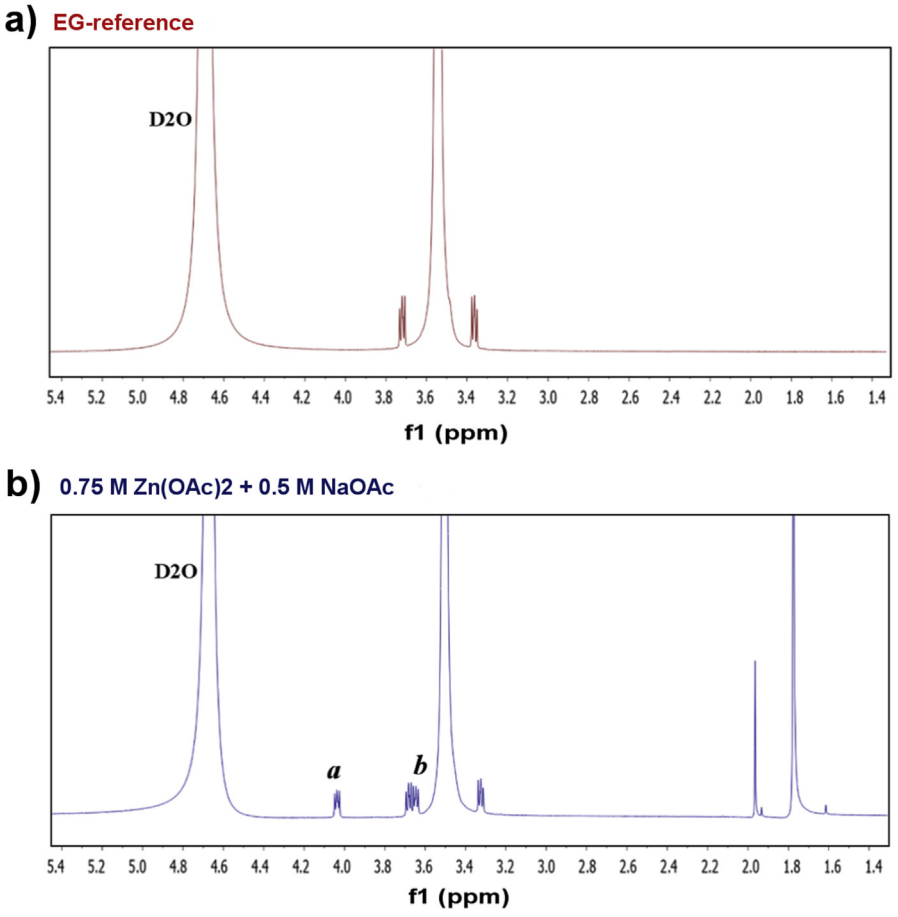

Fig. 1. ^{1}H NMR spectra. a) reference EG. b) EG complex where the glycol methylene signals proving the zinc complexation effect are labeled as a (4.06 ppm) and b (3.67 ppm).

experimental conditions. Deposits morphology dependence on current density and deposition potential was studied through scanning electron microscopy (SEM) (Zeiss EVO 50 EP) and energy dispersive spectroscopy (EDS) (Oxford instruments INCA x-sight detector). X-ray diffraction (XRD) (Philips model PW1830. $Ka1_{Cu}$ = 1.54058 Å) was adopted for the microstructural investiga-tion. Potentiodynamic polarization tests (1 mVs^{-1}) were conducted in 5 wt% NaCl aqueous solution after immersing the sample for 15 min. The solution (50 ml) was purged with nitrogen for 15 min with 40 L/h flux and during the test at 5 L/h to assure de-aerated conditions [41].

3. Results and discussion

3.1. Physical and electrochemical characterization

The use of acetate salts implies anionic species in the solution having a larger ionic radius than chlorides, normally present in DES. Hence, the lower conductivity values provided by the anionic species has to be balanced with a higher amount of metal precursor salt and, potentially, with the addition of a supporting electrolyte based on the same chemistry (e.g. acetates). Ethylene glycol containing zinc acetate (0.75 M) was not characterized by high conductivity (k = 0.55 mS cm^{-1} at 30 °C); moreover, for concentration of [$Zn(OAc)_2$]> 0.75 M, no further dissolution of the salt was observed and a white precipitate (ZnO) was likely to be formed. The addition of sodium acetate, [NaOAc] = 0.5 M, increased the elec-trolyte conductivity up to k = 1.33 mS cm^{-1} at 30 °C without compromising the cathodic efficiency of the electrodeposition process where no side cathodic reactions were addressed to sodium acetate degradation, together with a higher bath stability. The solution was then analyzed through ^1H NMR for the identification of complex species. In Fig. 1a, the spectrum of ethylene glycol showed the singlet signal at 3.53 ppm resulting from the four equivalent methylene protons and the characteristic satellite peaks at 3.72 ppm and 3.36 ppm related to the ^{13}C-^1H coupling, due to the low natural abundance of ^{13}C[42,43]. The interaction with zinc cations leading to the complex formation is showed in Fig. 1b where the appearance of signals "*a*" at 4.06 ppm and "*b*" at 3.67 ppm was representative of the methylene protons affected by the electronic interactions with Zn^{2+} promoting different chemical environment and resonance in the sample and resulting in a chemical shift of the peaks. The complex formation was strictly correlated to the Zn^{2+} effect considering that the chemical shift was not recognizable with the only use of Na^+; sodium acetate can be identified in the low ppm region of the spectrum (Fig. 1b) [44,45]. In aqueous and alcohol solutions $Zn(OAc)_2$ is able to reach an equilibrium state between its corresponding ions and the solvated salt [46]. The resulting Zn^{2+} interact with the EG terminal hydroxyl groups, considering the dissociation of the starting salt. On the other hand, sodium acetate can form Na^+ cations that are not reactive as Zn^{2+} to complex EG. Moreover, according to the experimental procedures, the number of used zinc acetate moles is higher than the sodium acetate one: as a result, the potential combination of Zn^{2+} with acetate anions provided by sodium acetate could be saturated, preserving however the availability of Zn^{2+} for EG complexes. Reduced formation of EG complex is observed in the complexation of diols using divalent metal ions, in the presence of anion auxiliary ligands, working in gas phase [47]. The formation of a zinc complex was also in agreement with the different increase in conductivity of ethylene glycol after the addition of a similar amount of sodium acetate and zinc acetate, where the former resulted to be more effective. The complexed zinc cations are characterized by a considerable steric hindrance with respect to sodium ones, with a minor contribution to the ionic conductivity.

Both the electrochemical characterization and electrodeposition were carried out at 70 °C to further increase the solution conductivity and to limit the water intake from the atmosphere. In the cyclic voltammetry (Fig. 2), the onset of zinc electrodeposition ($Zn^{2+} \longrightarrow Zn^0$) occurred at −0.94 V vs Pt corresponding to the sudden increase in the cathodic current; the linear dependence between cathodic potential and current density suggests that the process is kinetically controlled. In the reverse scan, a broad anodic peak ($Zn^0 \longrightarrow Zn^{2+}$) was detected whose recorded total charge indicated a high cathodic efficiency (CE >85%) if compared to the corresponding cathodic process. Linear sweep voltammetry (LSV) was carried out on mild steel at 5 mV s^{-1} with a lower cathodic limit (−4 V vs Pt). The same linear dependence noted in the CV was observed for relatively low cathodic overpotentials; conversely, the curve showed a broad reduction peak centered at −2 V vs Pt (Fig. 2). For cathodic potentials lower than −2.3 V vs Pt, secondary reactions due to either ethylene glycol deprotonation or residual water electrolysis, could take place. Despite the lack of significant secondary reactions, a small amount of hydrogen was expected also for lower overpotentials due to the presence of protons in solution. At

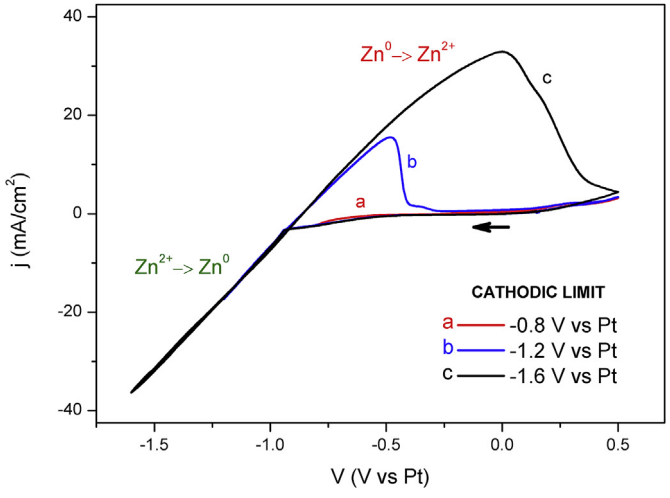

Fig. 2. Cyclic voltammetry of ethylene glycol solution containing 0.75 M zinc acetate and 0.5 M sodium acetate [70 °C, quiescent conditions, 20 mV s-1, WE: Pt].

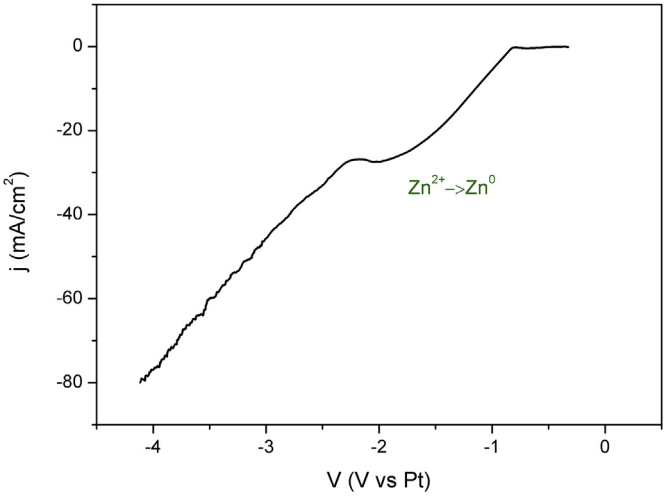

Fig. 3. Linear sweep voltammetry of ethylene glycol solution containing 0.75 M zinc acetate and 0.5 M sodium acetate [70 °C, quiescent conditions, 20 mV s-1, WE: mild steel].

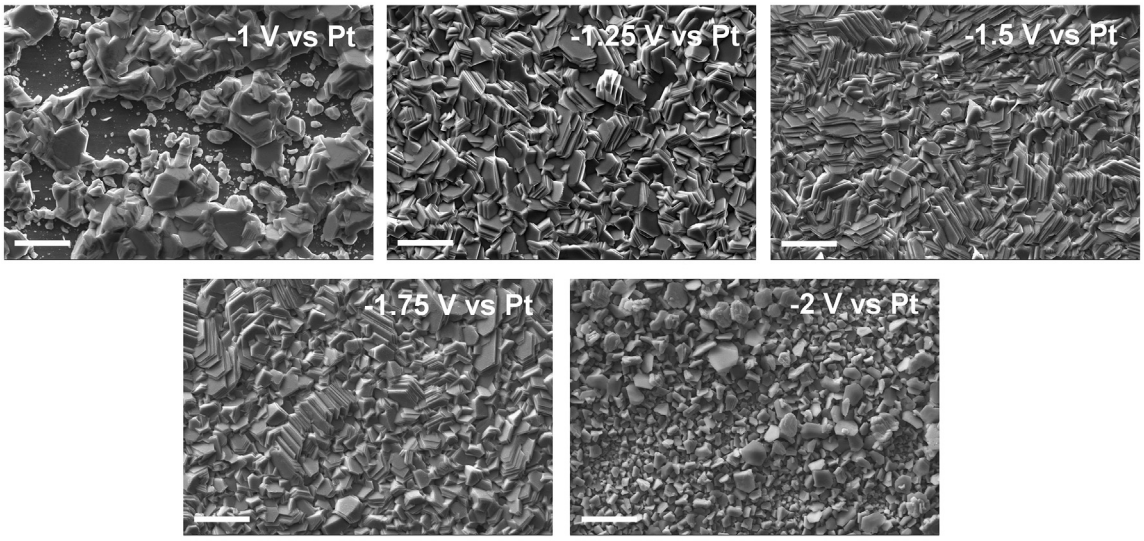

Fig. 4. SEM micrographs of zinc electrodeposits at different deposition potential from ethylene glycol solution containing 0.75 M zinc acetate and 0.5 M sodium acetate [70 °C, quiescent conditions, 20 mV s-1, WE: mild steel]. Scale bar: 10 μm.

the counter electrode, the formation of acetate byproducts was expected as reported in a previous work investigating the secondary reactions in a DES [10] where 1,2-ethanediol diacetate and ethanediol monoacetate were identified as anodic electrolysis byproducts when acetic acid was added [10]. In the present solution, no sign of degradation was detected after the electrochemical testing, however, the solution turned light yellow after carrying out electrodeposition for a few hours, suggesting the formation of byproducts. The use of a zinc sacrificial anode greatly reduced the color change, indicating that the majority of the anodic process was the dissolution of zinc electrode ($Zn^0 \longrightarrow Zn^{2+}$).

3.2. Potentiostatic deposition

Potentiostatic depositions were performed in the potential window ranging from − 1 V vs Pt to −2 V vs Pt according to the LSV (Fig. 3). The electrodeposition onset, observed at −0.94 V vs Pt from the electrochemical characterization (Figs. 2 and 3), was verified through potentiostatic depositions. At −0.9 V vs Pt no deposition occurred while, at −1 V vs Pt, an incomplete zinc film was formed due to the low applied overpotential (Fig. 4). Decreasing the cathodic potential to −1.75 V vs Pt, electrodeposition resulted in compact films with a hexagonal microstructure, also observed from the film morphology (Fig. 4). Secondary reactions started to have a significant role on film morphology at −2 v vs Pt, resulting in less compact and with a significant second order of roughness due to hydrogen bubbles pinning at the cathodic surface. Moreover, a consequent decrease in the faradaic efficiency from a maximum of CE ~85% (at −1.25 V vs Pt) to CE~60% was observed. On the other hand, no significant differences were perceived in both surface texture (Fig. 4) and current efficiency (Fig. 5a) from −1.25 V vs Pt to − 1.75 V vs Pt. In addition, an almost linear dependence between the deposition potential and the average current density was shown, resulting in relatively high values for an organic-based solution (Fig. 5b).

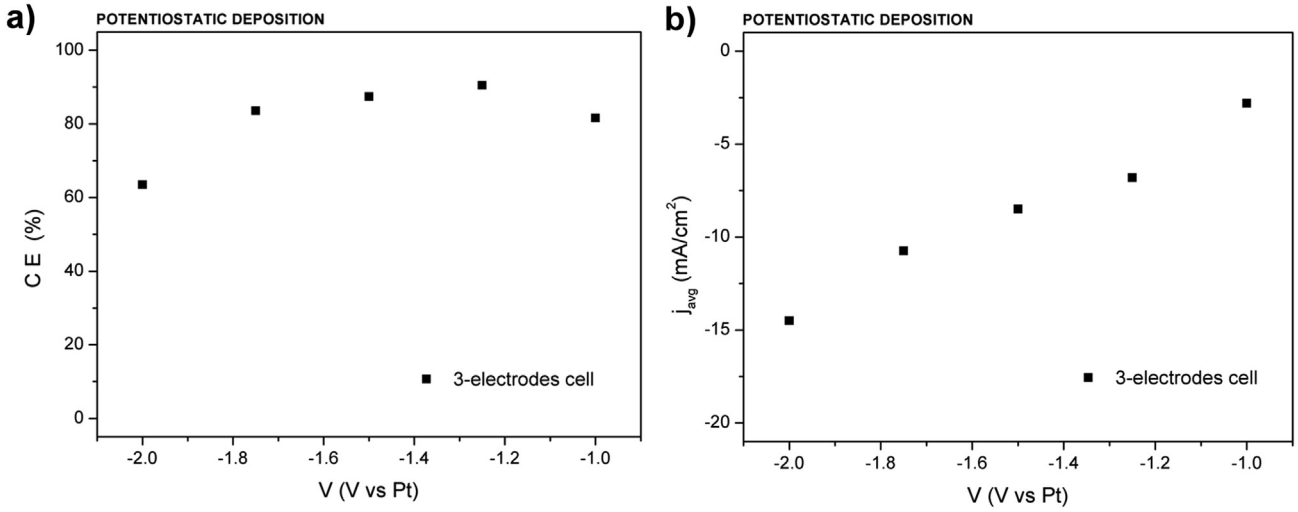

Fig. 5. a) Current efficiency (CE) dependence on the deposition potential. b) Corresponding average current density at the deposition potential.

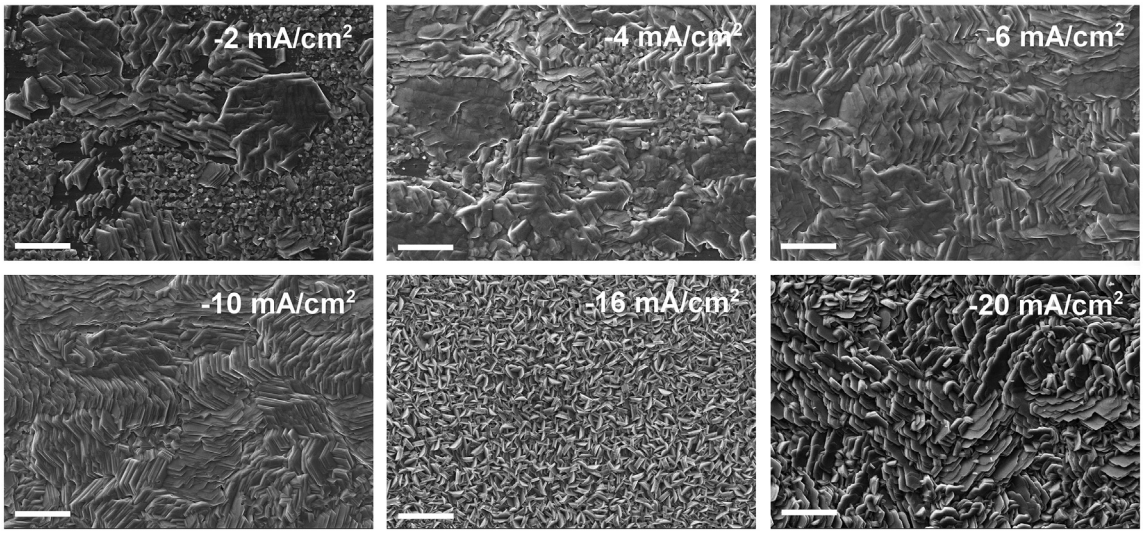

Fig. 6. SEM micrographs of zinc electrodeposits at different current densities resulting from the Hull cell test in ethylene glycol solution containing 0.75 M zinc acetate and 0.5 M sodium acetate [70 °C, quiescent conditions, 20 mV s-1, WE: mild steel]. Scale bar: 10 μm.

3.3. Hull cell study and galvanostatic deposition

Since the organic solutions were proposed as alternative to water-based ones also at the industrial level, a more practical approach was considered performing Hull cell tests. An unconventional glass cell (volume = 33 ml) was chosen where the current density distribution ranges from -1 mA/cm^2 to -20 mA/cm^2 applying a total cathodic current of I = -0.1 A according to the following empirical law indicated by the supplier (Eq. (1)):

$$\mathbf{C.D.} = \mathbf{I}[\mathbf{C}_1 - \mathbf{C}_2\mathbf{Log}(\mathbf{L})] \quad (1)$$

Where C.D. is the cathodic current density (A/dm^2), C_1 and C_2 are constants depending on electrolyte properties and L (cm) is the distance measured from the high-current side of the cathode. For the considered cell, $C_1 = 13.88$ and $C_2 = 20.55$ were the parameters indicated by the manufacturer. The test has been carried out for 10 min to assure a relevant film thickness for all the exploited current densities. In Fig. 6 the morphology dependence on the local deposition current density is shown: for the lowest value (-2 mA/cm^2), the substrate coverage was incomplete while, for higher current density values, compact zinc films were obtained. At the visual inspection, the coating on the Hull panel was characterized by a matt finish from -2 mA/cm^2 to -10 mA/cm^2, while for values higher than -16 mA/cm^2 the deposit was burnt.

After Hull test, galvanostatic deposition was also carried out in a conventional 2-electrodes cell considering current density values in agreement with the average ones recorded during the

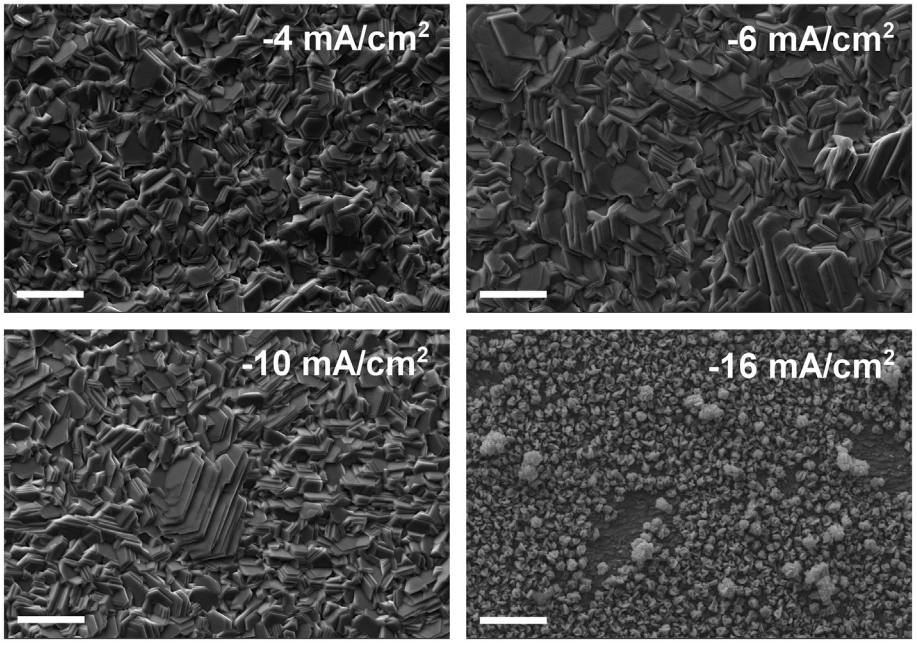

Fig. 7. SEM micrographs of zinc electrodeposits at different current densities from ethylene glycol solution containing 0.75 M zinc acetate and 0.5 M sodium acetate [70 °C, quiescent conditions, 20 mV s-1, WE: mild steel]. Scale bar: 10 μm.

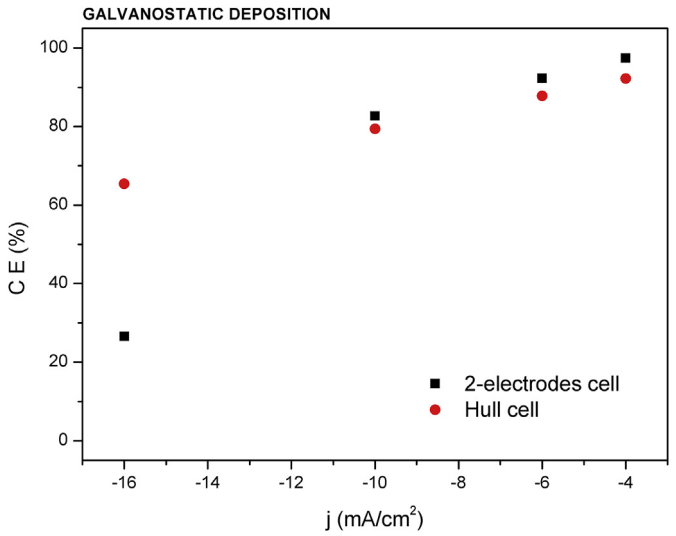

Fig. 8. Current efficiency (CE) dependence on the deposition current density for both standard 2-electrodes cell and Hull cell.

potentiostatic tests (Fig. 5b) and with the results of the Hull cell test (Fig. 6). As expected, from −4 mA/cm^2 to −10 mA/cm^2 zinc deposits were compact and homogeneous (Fig. 7) showing the same type of hexagonal features previously reported (Figs. 4 and 6). A discrepancy in the faradaic efficiency was found at −16 mA/cm^2, probably relying on the different approach in the measurement of the mole of material electrodeposited where in the case of conventional galvanic deposition was gravimetric (Fig. 8). The dendritic features of the film probably led to a higher error in the thickness measurement through XRF in case of Hull cell test (Fig. 6).

3.4. Film microstructure

Among all the experimental conditions, zinc deposits obtained from the potentiostatic deposition at −1.25 V vs Pt and the galvanostatic deposition at −6 mA/cm^2 were analyzed by X-rays diffraction (XRD). The diffractograms showed a significant orientation along the [002] direction (Fig. 9a,c), as also observed from the micrographs were the basal plane of the hexagonal cell could be clearly identified (Figs. 4, 6 and 7 and 9d). A more precise indication of the microstructural orientation is given by the relative texture coefficient (RTC), defined as follow (Eq. (2)):

$$RTC_{hkl} = \frac{I_{hkl}}{I_{0hkl}} \frac{n}{\sum_{i=1}^{n}\left(I_{hkl}/I_{0hkl}\right)} \quad (2)$$

Where the I_{hkl} is the relative diffraction intensity of a given plane

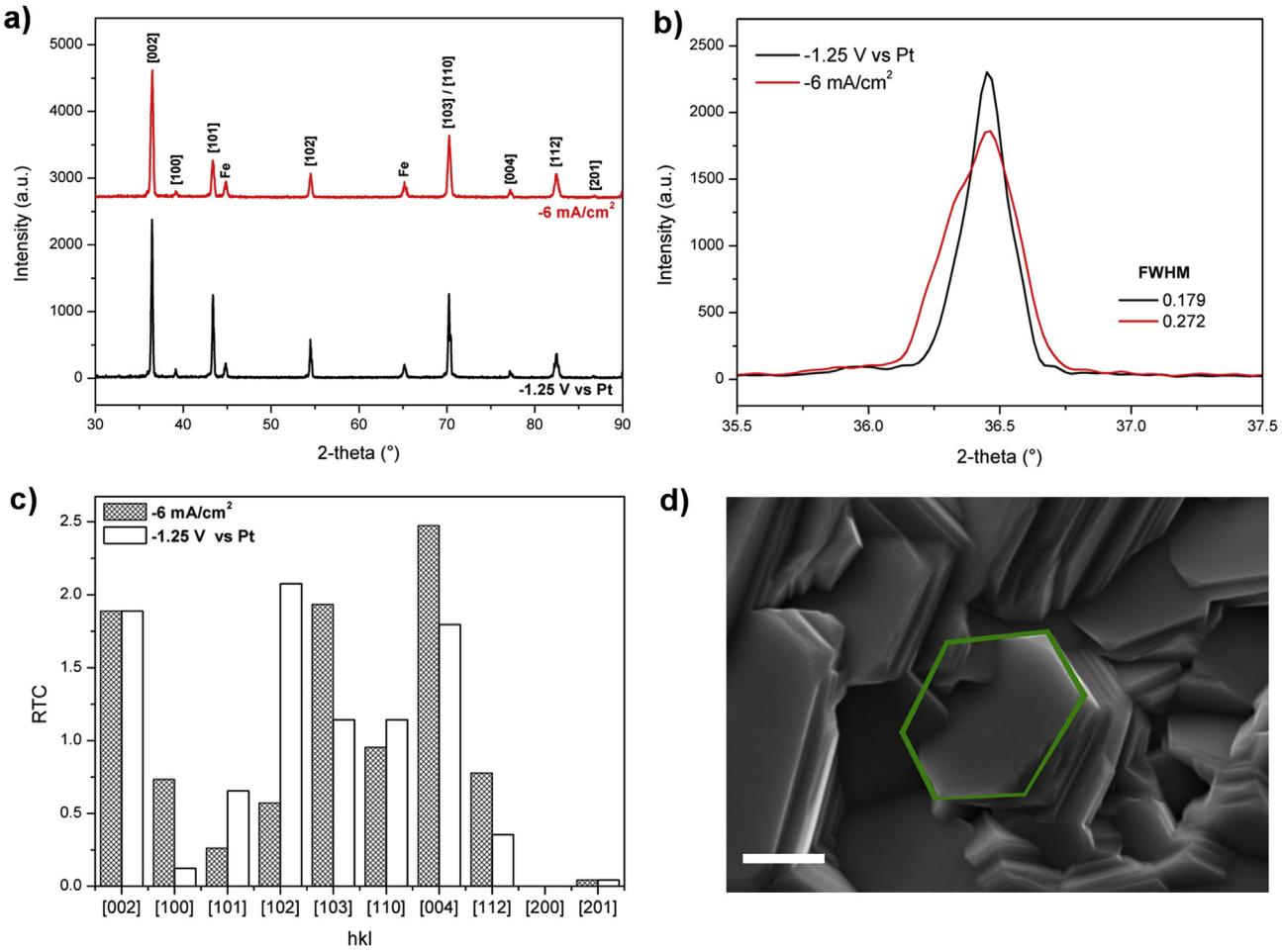

Fig. 9. a) XRD spectra of zinc electrodeposits by galvanostatic and potentiostatic approaches. b) (002) reflection with corresponding FWHM. c) Relative texture coefficient calculated from the peaks intensity from the XRD spectra and the standard relative diffraction intensity of the 04–0831 JCPDS. d) SEM micrograph of the zinc electrodeposit at −1.25 V vs Pt showing the basal plane tilted with respect to the orthogonal direction. Scale bar: 2 μm.

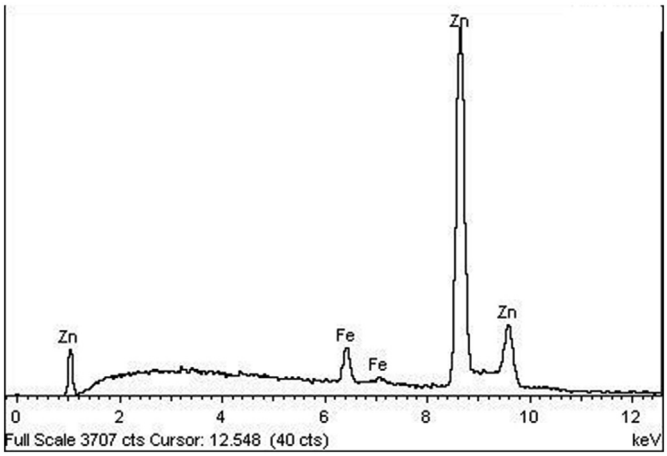

Fig. 10. EDS spectrum of a representative zinc deposit (GD: −6 mA/cm^2).

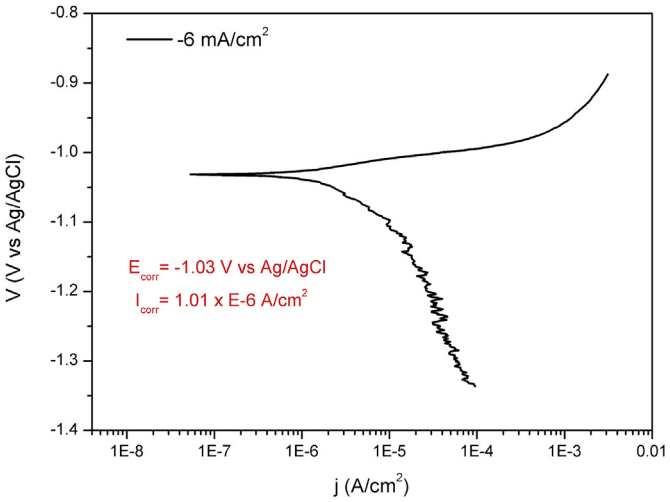

Fig. 11. Tafel plot of zinc coating (−6 mA/cm2) in de-aerated 5% wt. NaCl solution.

[hkl] measured experimentally, I_{0hkl} the standard diffraction intensity for the 04−0831 JCPDS (Joint Committee for Powder Diffraction Study). It showed the coexistence between [002]/[004] and [102] orientations (Fig. 9a) in accordance to the micrographs showing the presence of the basal plane (hexagonal shape) slightly tilted with respect to the orthogonal direction (Figs. 4, 6 and 7 and 9d). Electrodeposits with a preferential orientation along [002] direction were also observed on Pt(111)/Si substrate (Fig. S1), suggesting the electrolyte chemistry to be the main parameter affecting film growth. Both GD (−6 mA/cm^2) and PD (−1.25 V vs Pt) deposits were characterized by a similar texture (Fig. 9c); however, a difference in the full width at half maximum (FWHM) resulting in a different average crystallite size (τ) (Fig. 9b) was detected; the galvanostatic approach led to a smaller crystalline dimension. By applying the Debye-Scherrer equation, the galvanostatic deposit was characterized by $\tau = 32$ nm while for the potentiostatic one was $\tau = 49$ nm. The purity of the film obtained was also confirmed by electron dispersive spectroscopy (EDS) where no oxygen and carbon impurities were detected (Fig. 10).

3.5. Corrosion characterization

Polarization tests in de-aerated 5 wt % NaCl solutions were carried out to evaluate the corrosion behavior of the zinc coatings [48]. The dissolution mechanism normally involves the formation of insoluble oxides/hydroxides film [49], however, in presence of chlorides, this film does not influence the zinc dissolution because of its porous structure [50]. Considering the surface texture, the basal plane was expected to perform better against corrosion with respect to other surface orientations [51] together with a compact film morphology [48,52,53]. Fig. 11 shows the Tafel polarization plot for the zinc deposit obtained from the acetate-based ethylene glycol solution, resulting in an $E_{corr} = -1.03$ V vs Ag/AgCl and $I_{corr} = 1.01 \times 10^{-6}$ A/cm^2, in agreement with the results previously found for [002] oriented zinc coatings from aqueous solution [48]. Regarding the corrosion behavior of zinc electrodeposits from non-aqueous solutions, only few works reported the corrosion behavior of the coating showing similar or worse performances with respect to the present study ($E_{corr} = -1.02 \div -1.09$ V vs Ag/AgCl, $I_{corr} = 1.30-6.57 \times 10^{-6}$ A/cm^2 in 3% NaCl [30]; $E_{corr} = -1.05$ V vs Ag/AgCl, $I_{corr} \sim 4 \times 10^{-6}$ A/cm^2 in 3.5% NaCl [31]).

4. Conclusions

A chloride-free solution based on ethylene glycol containing acetate salts was proved to be suitable for the electrodeposition of high-quality zinc coatings. ^{1}NMR showed the formation of the zinc-ethylene glycol complex while no interaction between the solvent and sodium cations was observed, also proved by the effect of the two salts on bath conductivity. The electrochemical characterization showed the onset of zinc reduction around − 0.94 V vs Pt, resulting in high faradaic efficiency processes (>85%). However, the formation of acetate compounds at the counter electrode occurred for long-lasting electrodeposition experiments, where the use of a zinc sacrificial anode reduced greatly the electrolyte degradation. A wide potential interval (from − 1 V vs Pt to −2 V vs Pt) was investigated for the potentiostatic depositions resulting in a good match with the results from the LSV investigation. On the other hand, the galvanostatic experiments were supported by an investigation through Hull cell test showing a good agreement in terms of morphology and faradaic efficiency. The zinc deposits were compact, with no contamination and a pronounced preferential orientation along the [002]/[102] directions. A good corrosion behavior with a corrosion potential of $E_{corr} = -1.03$ V vs Ag/AgCl ($I_{corr} = 1.01 \times 10^{-6}$ A/cm^2) in de-aerated 5% NaCl aqueous solution was observed.

Appendix A. Supplementary data

Supplementary data to this article can be found online at https://doi.org/10.1016/j.electacta.2018.11.060.

References

[1] H. Geduld, Zinc Plating, ASM International, Trowbridge, 1988.
[2] X.G. Zhang, Corrosion and Electrochemistry of Zinc, Springer Science & Business Media, 2013.
[3] T. Welton, Room-temperature ionic liquids. Solvents for synthesis and catalysis, Chem. Rev. 99 (1999) 2071−2084, https://doi.org/10.1021/cr980032t.
[4] A.P. Abbott, D. Boothby, G. Capper, D.L. Davies, R.K. Rasheed, Deep eutectic solvents formed between choline chloride and carboxylic acids: versatile alternatives to ionic liquids, J. Am. Chem. Soc. 126 (2004) 9142−9147, https://doi.org/10.1021/ja048266j.
[5] Q. Zhang, K.D.O. Vigier, S. Royer, F. Jerome, Deep eutectic solvents: syntheses, properties and applications, Chem. Soc. Rev. 41 (2012) 7108−7146, https://doi.org/10.1039/C2CS35178A.
[6] E.L. Smith, A.P. Abbott, K.S. Ryder, Deep eutectic solvents (DESs) and their applications, Chem. Rev. 114 (2014) 11060−11082, https://doi.org/10.1021/cr300162p.
[7] R. Bernasconi, G. Panzeri, A. Accogli, F. Liberale, L. Nobili, L. Magagnin, Progress and Developments in Ionic Liquids, InTech, 2017, https://doi.org/10.5772/64935.
[8] K. Kumai, T. Ikeya, K. Ishihara, T. Iwahori, N. Imanishi, Y. Takeda, et al.,

Degradation mechanism due to decomposition of organic electrolyte in Li/MoS2 cells during long cycling, J. Power Sources 70 (1998) 235–239, https://doi.org/10.1016/S0378-7753(97)02678-5.
[9] M.C. Kroon, W. Buijs, C.J. Peters, G. Witkamp, Decomposition of ionic liquids in electrochemical processing, Green Chem. 8 (2006) 241–245, https://doi.org/10.1039/B512724F.
[10] K. Haerens, E. Matthijs, K. Binnemans, B. Van der Bruggen, Electrochemical decomposition of choline chloride based ionic liquid analogues, Green Chem. 11 (2009) 1357–1365, https://doi.org/10.1039/B906318H.
[11] S. Hsiu, J. Huang, I. Sun, C. Yuan, J. Shiea, Lewis acidity dependency of the electrochemical window of zinc chloride-1-ethyl-3-methylimidazolium chloride ionic liquids, Electrochim. Acta 47 (2002) 4367–4372, https://doi.org/10.1016/S0013-4686(02)00509-1.
[12] J. Yang, Y. Hsieh, T. Chu-Tien, I. Sun, Electrodeposition of distinct one-dimensional Zn biaxial microbelt from the zinc chloride-1-ethyl-3-methylidazolium chloride ionic liquid, J. Electrochem. Soc. 158 (2011) D235–D239, https://doi.org/10.1149/1.3559459.
[13] Z. Liu, N. Borisenko, S.Z. El Abedin, F. Endres, In situ STM study of zinc electrodeposition on Au (111) from the ionic liquid 1-ethyl-3-methylimidazolium trifluoromethylsulfonate, J. Solid State Electrochem. 18 (2014) 2581–2587, https://doi.org/10.1007/s10008-014-2516-x.
[14] J.S. Keist, C.A. Orme, P.K. Wright, J.W. Evans, An in situ AFM Study of the evolution of surface roughness for zinc electrodeposition within an imidazolium based ionic liquid electrolyte, Electrochim. Acta 152 (2015) 161–171, https://doi.org/10.1016/j.electacta.2014.11.091.
[15] Z. Liu, S. Zein El Abedin, N. Borisenko, F. Endres, Influence of an additive on zinc electrodeposition in the ionic liquid 1-ethyl-3-methylimidazolium trifluoromethylsulfonate, ChemElectroChem 2 (2015) 1159–1163, https://doi.org/10.1002/celc.201500108.
[16] D. Nieszporek, W. Simka, K. Matuszek, A. Chrobok, A. Maciej, Electrodeposition of zinc coatings from ionic liquid 227 (2015) 143–146.
[17] W. He, L. Shen, Z. Shi, B. Gao, X. Hu, J. Xu, et al., Zinc electrodeposition from zinc oxide in the urea/1-ethyl-3-methylimidazolium chloride at 353 K, Electrochemistry 84 (2016) 872–877, https://doi.org/10.5796/electrochemistry.84.872.
[18] Y. Chen, H. Yeh, N. Lo, C. Chiu, I. Sun, P. Chen, Electrodeposition of compact zinc from the hydrophobic Brønsted acidic ionic liquid-based electrolytes and the study of zinc stability along with the acidity manipulation, Electrochim. Acta 227 (2017) 185–193, https://doi.org/10.1016/j.electacta.2017.01.013.
[19] G. Pulletikurthi, M.S. Ghazvini, T. Cui, N. Borisenko, T. Carstens, A. Borodin, et al., Electrodeposition of zinc nanoplates from an ionic liquid composed of 1-butylpyrrolidine and ZnCl 2: electrochemical, in situ AFM and spectroscopic studies, Dalton Trans. 46 (2017) 455–464, https://doi.org/10.1039/C6DT04149C.
[20] Y. Wang, H. Yeh, Y. Tang, C. Kao, P. Chen, Voltammetric study and electrodeposition of zinc in hydrophobic room-temperature ionic liquid 1-butyl-1-methylpyrrolidinium bis ((trifluoromethyl) sulfonyl) imide ([BMP][TFSI]): a comparison between chloride and TFSI salts of zinc, J. Electrochem. Soc. 164 (2017) D39–D47, https://doi.org/10.1149/2.0451702jes.
[21] A. Abbott, J. Barron, K. Ryder, Electrolytic deposition of Zn coatings from ionic liquids based on choline chloride, Trans. IMF 87 (2009) 201–207, https://doi.org/10.1179/174591909X438857.
[22] A.H. Whitehead, M. Pölzler, B. Gollas, Zinc electrodeposition from a deep eutectic system containing choline chloride and ethylene glycol, J. Electrochem. Soc. 157 (2010) D328–D334, https://doi.org/10.1149/1.3364930.
[23] A.P. Abbott, J.C. Barron, G. Frisch, K.S. Ryder, A.F. Silva, The effect of additives on zinc electrodeposition from deep eutectic solvents, Electrochim. Acta 56 (2011) 5272–5279, https://doi.org/10.1016/j.electacta.2011.02.095.
[24] N.M. Pereira, P.M. Fernandes, C.M. Pereira, A.F. Silva, Electrodeposition of zinc from choline chloride-ethylene glycol deep eutectic solvent: effect of the tartrate ion, J. Electrochem. Soc. 159 (2012) D501–D506, https://doi.org/10.1149/2.004209jes.
[25] L. Vieira, A. Whitehead, B. Gollas, Mechanistic studies of zinc electrodeposition from deep eutectic electrolytes, J. Electrochem. Soc. 161 (2014) D7–D13, https://doi.org/10.1149/2.016401jes.
[26] H. Yang, R.G. Reddy, Electrochemical deposition of zinc from zinc oxide in 2: 1 urea/choline chloride ionic liquid, Electrochim. Acta 147 (2014) 513–519, https://doi.org/10.1016/j.electacta.2014.09.137.
[27] M. Starykevich, A. Salak, D. Ivanou, A. Lisenkov, M. Zheludkevich, M. Ferreira, Electrochemical deposition of zinc from deep eutectic solvent on barrier alumina layers, Electrochim. Acta 170 (2015) 284–291, https://doi.org/10.1016/j.electacta.2015.04.150.
[28] L. Vieira, R. Schennach, B. Gollas, The effect of the electrode material on the electrodeposition of zinc from deep eutectic solvents, Electrochim. Acta 197 (2016) 344–352, https://doi.org/10.1016/j.electacta.2015.11.030.
[29] S. Ibrahim, A. Bakkar, E. Ahmed, A. Selim, Effect of additives and current mode on zinc electrodeposition from deep eutectic ionic liquids, Electrochim. Acta 191 (2016) 724–732, https://doi.org/10.1016/j.electacta.2016.01.110.
[30] N.M. Pereira, C.M. Pereira, J.P. Araujo, A.F. Silva, Zinc Electrodeposition from deep eutectic solvent containing organic additives, J. Electroanal. Chem. 801 (2017) 545–551, https://doi.org/10.1016/j.jelechem.2017.08.019.
[31] Q. Bao, L. Zhao, H. Jing, A. Mao, Electrodeposition of zinc from low transition temperature mixture formed by choline chloride lactic acid, Mater. Today Commun. 14 (2018) 249–253, https://doi.org/10.1016/j.mtcomm.2018.01.015.
[32] G. Panzeri, M. Tresoldi, C. Rinaldi, L. Magagnin, Electrodeposition of magnetic SmCo films from deep eutectic solvents and choline chloride-ethylene glycol mixtures, J. Electrochem. Soc. 164 (2017) D930–D933, https://doi.org/10.1149/2.0111714jes.
[33] G. Panzeri, A. Accogli, E. Gibertini, C. Rinaldi, L. Nobili, L. Magagnin, Electrodeposition of high-purity nanostructured iron films from Fe (II) and Fe (III) non-aqueous solutions based on ethylene glycol, Electrochim. Acta 271 (2018) 576–581, https://doi.org/10.1016/j.electacta.2018.03.174.
[34] R. Böck, S. Wulf, Electrodeposition of iron films from an ionic liquid (ChCl/urea/FeCl3 deep eutectic mixtures), Trans. IMF 87 (2009) 28–32, https://doi.org/10.1179/174591908X379601.
[35] T. Vorobyova, O. Vrublevskaya, Electrochemical deposition of gold–tin alloy from ethylene glycol electrolyte, Surf. Coating. Technol. 204 (2010) 1314–1318, https://doi.org/10.1016/j.surfcoat.2009.10.010.
[36] H.P. Nguyen, M. Wu, J. Su, R.J. Vullers, P.M. Vereecken, J. Fransaer, Electrodeposition of bismuth telluride thermoelectric films from a nonaqueous electrolyte using ethylene glycol, Electrochim. Acta 68 (2012) 9–17, https://doi.org/10.1016/j.electacta.2012.01.091.
[37] M. Wu, H.P. Nguyen, R.J. Vullers, P.M. Vereecken, K. Binnemans, J. Fransaer, Electrodeposition of bismuth telluride thermoelectric films from chloride-free ethylene glycol solutions, J. Electrochem. Soc. 160 (2013) D196–D201, https://doi.org/10.1149/2.089304jes.
[38] J. Wellings, A. Samantilleke, S. Heavens, P. Warren, I. Dharmadasa, Electrodeposition of CuInSe2 from ethylene glycol at 150° C, solar energy mater, Sol. Cell. 93 (2009) 1518–1523, https://doi.org/10.1016/j.solmat.2009.03.031.
[39] H. Maltanava, T. Vorobyova, O. Vrublevskaya, Electrodeposition of tin coatings from ethylene glycol and propylene glycol electrolytes, Surf. Coating. Technol. 254 (2014) 388–397, https://doi.org/10.1016/j.surfcoat.2014.06.049.
[40] M. Pallaro, F. Moretto, G. Panzeri, L. Magagnin, Sn-Cu codeposition from a non-aqueous solution based on ethylene glycol for wafer-bonding applications: direct and pulse electroplating, Trans. IMF 96 (2018) 265–268, https://doi.org/10.1080/00202967.2018.1507329.
[41] I.B. Butler, M.A. Schoonen, D.T. Rickard, Removal of dissolved oxygen from water: a comparison of four common techniques, Talanta 41 (1994) 211–215, https://doi.org/10.1016/0039-9140(94)80110-X.
[42] B.R. Dauner, D.L. Pringle, Proton NMR analysis of heat exchange fluids containing ethylene glycol, propylene glycol, and water: a real-world experiment for the analytical laboratory, J. Chem. Educ. 91 (2014) 743–746, https://doi.org/10.1021/ed400649f.
[43] M.L. Harrell, D.E. Bergbreiter, Using ^{1}H NMR spectra of polymers and polymer products to illustrate concepts in organic chemistry, J. Chem. Educ. 94 (2017) 1668–1673, https://doi.org/10.1021/acs.jchemed.6b00801.
[44] J. Shin, Y. Kim, Y.M. Lim, Y.C. Nho, Removal of sodium acetate in poly (vinyl alcohol) and its quantification by 1H NMR spectroscopy, J. Appl. Polym. Sci. 107 (2008) 3179–3183, https://doi.org/10.1002/app.27453.
[45] M. Rajabzadeh, Determination of unknown concentrations of sodium acetate using the method of standard addition and proton NMR: an experiment for the undergraduate analytical chemistry laboratory, J. Chem. Educ. 89 (2012) 1454–1457, https://doi.org/10.1021/ed200577v.
[46] G.R. Gattorno, G. Oskam, Forced hydrolysis vs self-hydrolysis of zinc acetate in ethanol and iso-butanol, ECS Trans. 3 (2006) 23–28, https://doi.org/10.1149/1.2357093.
[47] P.J. Ruttink, L.J. Dekker, T.M. Luider, P.C. Burgers, Complexation of divalent metal ions with diols in the presence of anion auxiliary ligands: zinc-induced oxidation of ethylene glycol to glycolaldehyde by consecutive hydride ion and proton shifts, J. Mass Spectrom. 47 (2012) 869–874, https://doi.org/10.1002/jms.3039.
[48] S. Khorsand, K. Raeissi, M. Golozar, An investigation on the role of texture and surface morphology in the corrosion resistance of zinc electrodeposits, Corros. Sci. 53 (2011) 2676–2678, https://doi.org/10.1016/j.corsci.2011.04.007.
[49] R. Krishnan, C. Kennedy, S. Jayakrishnan, S. Sriveeraraghavan, S. Natarajan, C. Ramamurthy, et al., Zinc electrodeposition from acetate solutions, Met. Finish. 94 (1996) 43–46.
[50] R. Ramanauskas, Structural factor in Zn alloy electrodeposit corrosion, Appl. Surf. Sci. 153 (1999) 53–64, https://doi.org/10.1016/S0169-4332(99)00334-7.
[51] H. Park, J. Szpunar, The role of texture and morphology in optimizing the corrosion resistance of zinc-based electrogalvanized coatings, Corros. Sci. 40 (1998) 525–545, https://doi.org/10.1016/S0010-938X(97)00148-0.
[52] M. Mouanga, L. Ricq, J. Douglade, P. Berçot, Corrosion behaviour of zinc deposits obtained under pulse current electrodeposition: effects of coumarin as additive, Corros. Sci. 51 (2009) 690–698, https://doi.org/10.1016/j.corsci.2008.12.020.
[53] D. Vasilakopoulos, M. Bouroushian, N. Spyrellis, Electrocrystallisation of zinc from acidic sulphate baths; A nucleation and crystal growth process, Electrochim. Acta 54 (2009) 2509–2514, https://doi.org/10.1016/j.electacta.2008.11.059.